

CRYSTALLIZATION FOULING ON COATINGS OF TITANIA AND TITANIA-FLUOROALKYLSILANE DURING NUCLEATE BOILING

Y.W. Cai¹ and M.Y. Liu^{1,2*}

¹ School of Chemical Engineering and Technology, Tianjin University, Tianjin 300072, China and E-mail (Corresponding author: myliu@tju.edu.cn)

² State Key Laboratory of Chemical Engineering, Tianjin 300072, China

ABSTRACT

The micro-nanometer titania coatings as well as the hydrophobic titania-fluoroalkylsilane composite coatings were prepared on the polished 304 type stainless steel discs by liquid phase deposition method. Surface morphology and chemical elements of the coatings were analyzed by field emission scanning electron microscopy and X-ray photoelectron spectroscopy. Transparent coating thickness was measured by non-contact optical film thickness instrument. Contact angle of coating surface was measured with video optical contact angle measuring instrument and surface free energy was calculated. A pool boiling apparatus with online data acquisition system was established to evaluate the heat transfer and fouling performances of the coatings. Pool boiling and fouling experiments on the coated surfaces were carried out with the heat flux of $123.6 \text{ kW}\cdot\text{m}^{-2}$ and the initial calcium carbonate concentration of $250 \text{ mg}\cdot\text{L}^{-1}$. The results show that thinner coatings enhance heat transfer coefficients of pool boiling but thicker coatings reduce them greatly, especially in higher heat fluxes; asymptotic type of fouling curve is obtained. The hydrophobic titania-fluoroalkylsilane composite coatings are favorable for pool boiling heat transfer as well as for inhibiting fouling.

INTRODUCTION

Fouling is the undesirable forming deposition on the heat transfer surface. Pool boiling is one of the most efficient means in thermal transfer process. The fouling in pool boiling is severe because of the high surface temperature, the bubble behaviors, and the rapid super-saturation of salts with inverse solubility. To minimize fouling formation and enhance heat transfer, one of the strategies is surface coating. Zhao et al. (Zhao and Liu, 2004; Zhao and Wang, 2005; Zhao and Liu et al., 2005) studied the antifouling properties of the Ni-Cu-P-PTFE coating and the F-diamond-like carbon (DLC) film in CaSO_4 solution, as well as the anti-bacterial fouling of the Ni-Cu-P-PTFE coating. They derive the optimum surface free energy theory using the XDLVO theory and conclude that the surface with the optimum surface free energy has the minimal deposit adhesion. Malayeri et al. (2009) performed the calcium sulphate scale

tests on the micrometer-thickness of the nano-structured K-S coating series with the spike-shaped, hydrophobic nano-structured surfaces. The test results demonstrate that these coatings significantly increase the induction time and decrease the fouling rate compared with the untreated AISI 304 BA stainless steel surface. The TiO_2 coating was applied to enhance heat transfer as well as reduce fouling depositions. Wang et al. (2007) prepared the TiO_2 coatings on copper substrate with different layer coating thickness in nanometer scale by using the vacuum coating technique. The results show that all the TiO_2 coating surfaces can avoid fouling deposition. However, the concentration of the CaCO_3 fouling solution is very low. Recently, Al-Janabi et al. (2009, 2011) investigated the influence of the solvent based, the water based, and the electroless Ni-P-BN coatings on the interaction energies between CaSO_4 deposits and the modified surfaces. The results show that the surface with higher electron donor component produces higher repulsive energy and greater reduction of the adhesion force between the surface and the deposits. Fluoroalkylsilane (FPS) was often used to prepare the hydrophobic as well as the super-hydrophobic coatings (Nishino et al., 1999; Sermon et al., 2004; Lai et al., 2009). So it is feasible to reduce the free energy of the heat transfer surface by modification of the coatings with FPS. However, Takata et al. (2006) found that the film boiling occurs easily on the super-hydrophobic surface, which is harmful to heat transfer. So the moderate wettability of the heat transfer surface might be available both for pool boiling enhancement and fouling prevention. In this work, heat transfer and crystallization fouling behaviors on TiO_2 and TiO_2 -FPS composite hydrophobic coatings were investigated on the plain disc during pool boiling.

EXPERIMENTAL

Preparation of TiO_2 -FPS composite coatings

The substrate was AISI304 type stainless steel (SS). Titania coatings were prepared by liquid phase deposition (LPD) method on the metallic disks of the SS substrates with the diameter of 180 mm and the thickness of 6 mm. TiO_2 coated disks were dipped into the FPS-17 (Tianjin

Yonglong Technology Development Co., Ltd., China) hydrophobic solution to decrease the surface energy of the coatings. Then the disk was heat treated. Four TiO₂ coatings (A, B, C and D) with varied film thickness were prepared on the polished SS substrates. The coatings B, C and D were also treated with FPS hydrophobic solution, which were named after BF, CF and DF, respectively. The polished SS was prepared for comparison tests.

Preparation of calcium carbonate solution

Calcium carbonate solution was prepared by mixing a certain quantity of calcium chloride (CaCl₂) and sodium bicarbonate (NaHCO₃) in deionized water with temperature of 293 K. The molar ratio of the former to the latter is 0.5. The solution concentration was measured with the ethylenediamine-tetra-acetic-acid (EDTA) titration using the calcium-carboxylic acid indicator. The initial concentration of calcium carbonate solution is 250 mg·L⁻¹. The initial pH value of the fouling solution is 8.42 ± 0.29, which was measured by the portable pH meter (PHB-4, Shanghai Precision Scientific Instrument, China). In order to minimize the loss of the foulant in the boiling solution and compensate the amount of the steam condensate from the exit of the pool boiling device, the same volumes of the CaCO₃ solution were injected very slowly into the boiling pool every half hour.

The pool boiling apparatus

The schematic diagram of the apparatus is largely the same as that in literature except that the cylinder cooper heater was mounted horizontally as the heat source with one end contacts with the boiling disk (Wang et al., 2007). The pool boiling and the fouling tests were carried out in the nucleate boiling state at atmospheric pressure. To maintain relatively stable concentration of the fouling solution, the same volumes of the CaCO₃ solution were injected into the boiling pool every one hour according to the amount of the steam condensate from the export of the pool boiling device.

Error and uncertainty analysis

The maximum uncertainty for measuring the heat flux is 5.15%. The vapor pressure has been measured with the pressure vacuum gauge. The factory calibrated expanded uncertainty is estimated to be 1.5% of the operating range with 95% confidence. All of the five thermocouples have been calibrated with the second standard precision mercury thermometer with the accuracy of ±0.01 K to eliminate the systematic error. After calibration, the thermocouples do not exceed the measurement error of ±0.2 K. The maximum error for the heat transfer coefficients evaluation is about 6.69%. The average heat loss of the apparatus in the course of the experiments is 6.42%.

RESULTS AND DISCUSSION

Coating thickness measurement

The TiO₂ coating thickness was gauged with the thin film thickness measuring instrument which uses a non-contact

optical evaluation measurement technology. The thickness of the coatings A, B, C, and D are 63.8 ± 0.5 nm, 104.7 ± 0.5 nm, 159.1 ± 2.5 nm, and 204.9 ± 2.8 nm, respectively.

Field emission scanning electron microscopy

The morphology and the elemental distribution of the TiO₂ coatings were analyzed by the field emission scanning electron microscopy (FE-SEM, Nanosem 430, FEI Corp., USA). Figure 1 shows the plan view FE-SEM images of the polished SS, the TiO₂ coatings, and the TiO₂-FPS composite coating, respectively. The coating A consists of many large TiO₂ nano-crystals. The coatings B and C consist of porous grains with a few tens of nanometers in size. The coating C is denser than the coating B. These nano-holes might be available for the nucleation sites of bubbles during pool boiling process. The coating D consists of many large and dense micro-particles, and almost no pores are found on this surface. These micro-particles might provide the crystal cores for the fouling deposition. The coating CF becomes denser compared with the coating C.

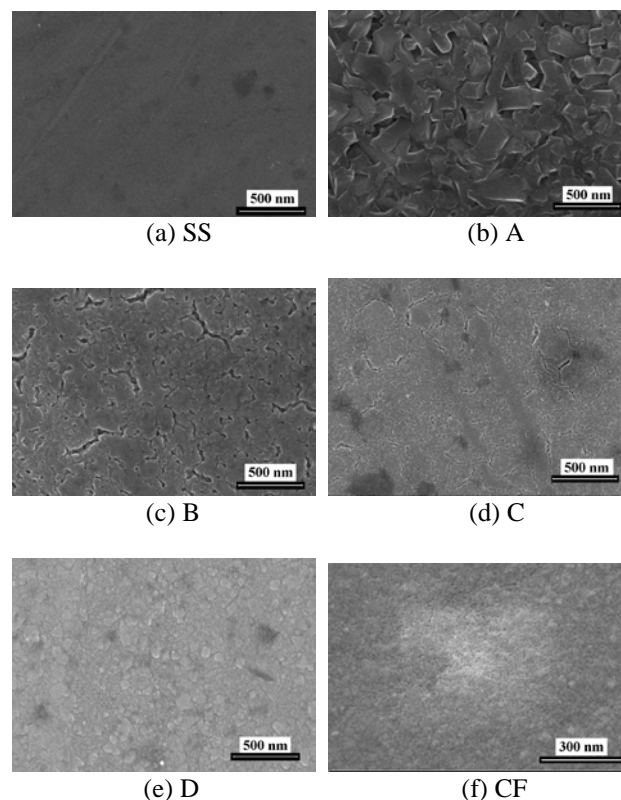


Fig. 1 Plan view FE-SEM images of the polished SS, TiO₂, and TiO₂-FPS coating surfaces; (a) polished SS; (b), (c), (d), and (e) TiO₂ coating with varied film thickness; (f) TiO₂-FPS composite coating.

XPS measurement

The TiO₂ thin coating was analyzed by X-ray photoelectron spectroscopy (XPS) device (PHI 1600 ESCA, Perkin-Elmer Co., USA). For the coating B, the percentage of Ti and O element in this coating is 25.2% and 56.1%, respectively. The number ratio of O and Ti is 2.23, which is slightly higher than the atomic stoichiometry of the TiO₂

compound. The titanium element in the coating not only possesses Ti (IV), but also Ti (II) and Ti (III). 43.3% (atom percent) of the Ti (IV) in the coating reduces to lower chemical valence. For the hydrophobic coating BF, the chemical bonds of CF₂, CF₃, Si-C, and Si-O are found in the XPS survey spectrum.

Surface free energy calculation

The contact angles of the heat transfer surfaces were measured using the sessile drop method (Michalski et al., 1998) with the video optical contact angle measuring instrument (OCA20, DataPhysics Instruments GmbH, Filderstadt, Germany) at 293±1 K. Each injection volume of standard liquid was 2 µL. The standard liquids used were water (doubly distilled), formamide and diiodomethane. Each standard liquid was used as received and with no further treatment.

Surface roughness measurement

The surface texture profile was measured with the JB-8C Roughness Tester. The results of the surface roughness and calculated surface free energy by contact angles are shown in Fig. 2. Figure 2 shows that the surface roughness of the SS surface is very low, but the surface free energy is relatively high. The coating A with the least nano-scale titania thickness has larger surface roughness and higher surface free energy. The surface roughness as well as the surface free energy increases with the increase of the coating thickness with regard to the coatings of B, C and D. However, the reason for the correlation between the surface properties and the coating thickness is not clear. The surface free energy of the TiO₂ coating decreases sharply when treated with the FPS hydrophobic solution. But the surface roughness does not change too much. The reason is that the FPS hydrophobic film is of the self-assembled monolayer, which has little effect on the surface morphology.

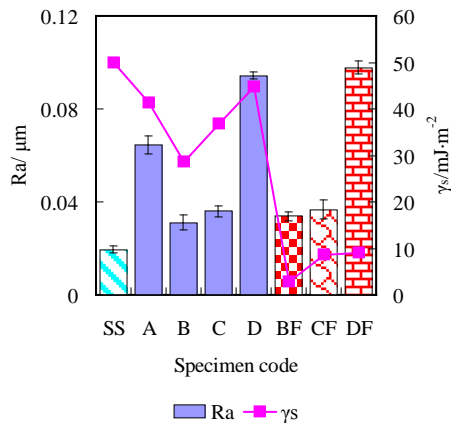
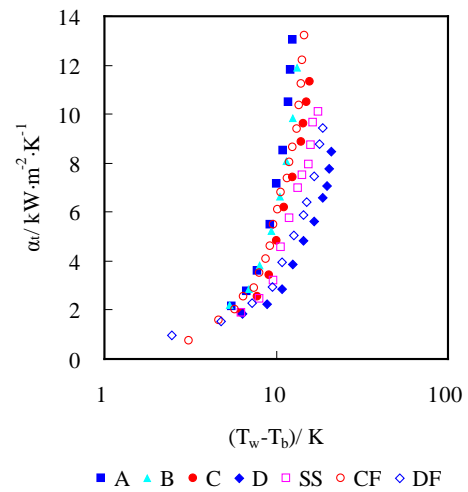


Fig. 2 Surface roughness and surface free energy of the different surfaces. (SS: AISI304 stainless steel; A, B, C, and D: TiO₂ coating; BF, CF, and DF: TiO₂-FPS composite coating).

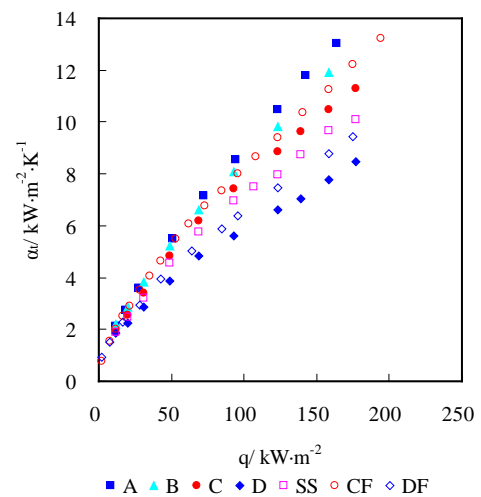
Pool boiling experiments

Figure 3 shows the variation of the heat transfer coefficient with the heat flux for pool boiling of deionized water on the coatings of A, B, C, and D as well as the

hydrophobic composite coatings of CF and DF. For comparison, the results for the polished SS surface are also shown in this figure. Figure 4 shows the percentage change of the heat transfer coefficient on the coatings compared with SS substrate at different heat fluxes. The results indicate that the coatings of A, B and C improve the pool boiling heat transfer coefficients obviously, especially in higher heat flux, compared with the polished SS surface. These three coatings with nano-particles have larger surface roughness than that of the polished SS, as shown in Fig. 2. Meanwhile, there are many nano-scale cavities on these three surfaces which could provide nucleation sites for pool boiling. Since the rougher surface has more nucleated sites for bubble formation, its heat transfer coefficient is higher than that of the polished SS surface.



(a) Boiling coefficient versus superheat degree



(b) Heat transfer coefficient versus heat flux

Fig. 3 Pool boiling heat transfer coefficients on various heat transfer surfaces. (SS: AISI304 stainless steel; A, B, C, and D: TiO₂ coating; BF, CF, and DF: TiO₂-FPS composite coating).

An increase in the coating thickness from 63.8±0.5 nm to 159.1 ± 2.5 nm decreases the heat transfer coefficients, as

shown in Fig. 3. However, the heat transfer coefficients are deteriorated when the polished SS surface coated with TiO₂ with the thickness of 204.9 ± 2.8 nm (coating D). Because the thermal conductivity of the TiO₂ substance is only about half that of the 304SS at 400K, such a thick and dense coating with low thermal conductivity would partially offset the advantage of enhanced heat transfer due to the surface micro-roughness of the TiO₂ coating and so leads to slightly inhibit the heat conduction of the surface.

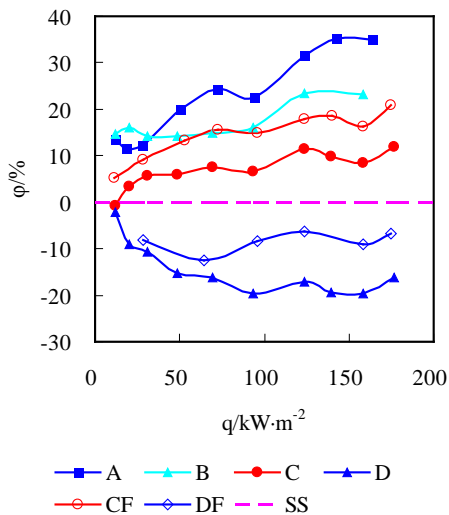


Fig. 4 Percentage change of heat transfer coefficient on coatings compared with SS substrate at different heat fluxes; A, B, C, and D: TiO₂ coating; CF and DF: TiO₂-FPS composite coating; SS: AISI304 stainless steel.

The heat transfer coefficients on all the TiO₂-FPS composite coatings increase after the TiO₂ coatings with hydrophobic treatments. It is generally recognized that there are three main mechanisms contributing to nucleate boiling heat transfer: the bubble generation and departure from nucleation sites on the superheated surface, micro-layer evaporation underneath the bubbles, and natural convection on inactive nucleation areas of the heated surface (Yu, et al., 2002; Chu, et al., 2009). Heat transfer contribution due to the first two categories (heat flux of evaporation latent) account for approaches 90% of the total heat flux at high heat flux (Chu, et al., 2009). It is considered that the boiling heat transfer coefficient has a positive relationship with the active nucleation site density (Wang et al., 1993). Moreover, the work required for vapor bubbles creation on the hydrophobic surface is very small, so the boiling bubbles are more likely generated on this surface (Liang et al., 1998; Piore et al., 2004). Eventually, more bubble sites are observed on the heating surface and higher heat transfer coefficient is available when boiling occurs on the TiO₂-FPS composite coating.

The heat transfer coefficient of the hydrophobic coating DF is still lower than that of SS surface at the same heat flux although it has very low surface free energy. The result indicates that there is a competition on the contribution of the heat transfer coefficient between the surface energy and the coating thickness. Low surface free energy promotes the

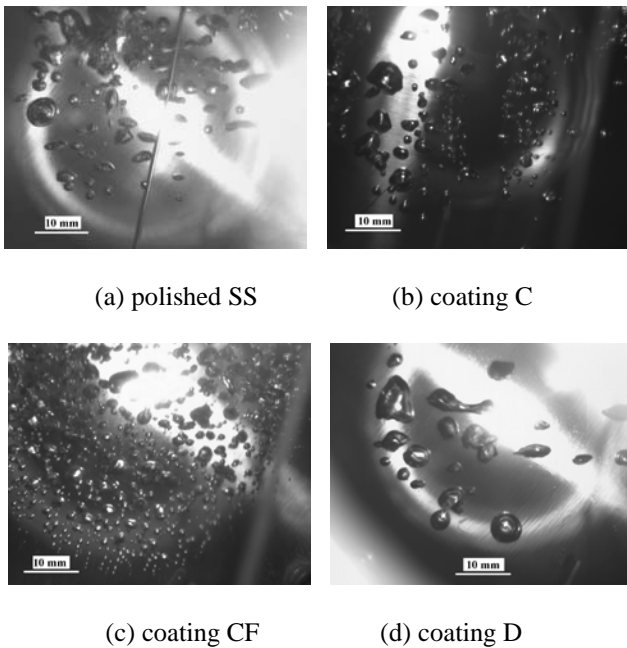
number of bubbles formation on the surface; however, the thick coating with low thermal conductivity would provide the additional thermal resistance and partially inhibit the heat transfer. The surface roughness of the coatings C and CF has little difference, but the coating CF with low surface energy improves the pool boiling heat transfer coefficient clearly. In brief, the factors of surface free energy, surface roughness, materials, as well as surface nano-morphology should be considered comprehensively for pool boiling heat transfer enhancement.

The typical single frame of boiling photographs with CMOS camera (BASLER A504k, 500-1000fps, Germany) on the surface of SS, C, CF and D at heat flux of $123.6 \text{ kW}\cdot\text{m}^{-2}$ are shown in Fig. 5, respectively. The average departure diameter on the heat surface was statistically calculated with Image-Pro Plus software (version 6.0, Media Cybernetics, Inc., USA). The bubble waiting and growth time were estimated and calculated according to the image sequences of the bubbles. No less than five bubble sites on the heat transfer surface and no fewer than three sequences for each bubble were chosen to calculate the bubble parameters. The results of the bubble dynamic parameters on these surfaces are shown in Table 1. The results show that the nucleation site density on the coating CF is far greater than that on other surfaces during the pool boiling tests. The diameters of the boiling bubbles are small and the bubble sites distribute uniformly on this surface, as shown in Fig. 5(c). The frequency of bubbles departure is about 84 bubbles per second, which is the highest value on all of the heat transfer surfaces in this paper. The large nucleation sites density, the small size bubbles as well as the high bubble departure frequency might benefit the enhancement of the heat transfer of the coating CF. In addition, the average growth time, \bar{t}_g , is double of the waiting time, \bar{t}_w .

The rule of the bubble dynamics on the coating CF is similar to that on the low energy surface of Teflon in the literature (Rankin, et al., 1973). There are fewer bubble formation sites and the vapor bubbles with large departure diameters are observed on coating D as shown in Fig. 5(d). The average departure diameter of the bubbles is 4 mm and the detachment frequency is about 14 bubbles per second, which is lower than that on other surfaces. The average waiting time is about 1.5 times as long as the growth time during the bubbles formation and growth process on the coating D surface. This means that the convection form takes more than half of the total time of heat transfer process on the single bubble formation site. Moreover, such a low detachment frequency and long waiting time of the bubbles is detrimental to the pool boiling heat transfer. The average departure diameter of bubbles on the coating C surface is about 1.8 mm, and the departure frequency is about 35 bubbles per second which is larger than that on the SS surface. It is surprising that the growth time of the bubbles is equal to the waiting time on coating C surface. However, the waiting time of bubbles on SS surface is about 3 times as long as the growth time. Another boiling phenomenon observed is that the boiling bubbles formation and growth are always at the fixed nucleate sites (not random distribution) throughout the pool boiling process. The

bubbles on the heat transfer surface with larger departure diameter might have a longer waiting time and lower departure frequency as shown in Table 1.

In addition, the bubble shape on the coating CF surface is hemispherical while the shape on the D surface is oblate, as shown in Figs. 5(c) and (d). According to the literature (Johnson et al., 1966; Jamialahmadi et al., 1989), the shapes of departure bubbles are controlled by the surface tension force and the inertial force. When the surface tension forces dominate the departure, the bubbles tend to be spherical. However, when the inertial forces dominate the bubbles tend to be hemispherical, and when both forces are significant the bubbles have an oblate shape.



(a) polished SS

(b) coating C

(c) coating CF

(d) coating D

Fig. 5 The typical photograph of boiling phenomena of deionized water on different disk surfaces with the heat flux of $123.6 \text{ kW}\cdot\text{m}^{-2}$.

Table 1 Bubble dynamics on different heating surfaces

Code	\bar{D}_d/mm	\bar{f}/Hz	$\bar{\tau}_g/\text{ms}$	$\bar{\tau}_w/\text{ms}$	$(\bar{\tau}_g + \bar{\tau}_w)/\text{ms}$
SS	2.7 ± 0.5	24.8 ± 0.9	9.6 ± 0.9	30.8 ± 1.0	40.4 ± 0.9
C	1.8 ± 0.3	34.5 ± 0.6	14.5 ± 0.5	14.5 ± 0.8	29.0 ± 0.6
CF	0.8 ± 0.1	83.3 ± 0.2	8.0 ± 0.1	4.0 ± 0.2	12.0 ± 0.2
D	4.0 ± 0.8	12.3 ± 1.1	32.2 ± 1.1	48.9 ± 1.0	81.1 ± 1.0

Fouling experiments

The fouling tests were carried out with seven different discs, i.e., three TiO_2 coatings with varied thickness (B, C, and D), three TiO_2 -FPS composite hydrophobic coatings (BF, CF, and DF) and one polished SS surface. The initial concentration of calcium carbonate was $250 \text{ mg}\cdot\text{L}^{-1}$ and the heat flux is $123.6 \text{ kW}\cdot\text{L}^{-1}$.

Figure 6 shows the fouling resistances versus time on these seven heat transfer surfaces. The asymptotic fouling resistances calculated from Fig. 6 are plotted in histogram form, as shown in Fig. 7.

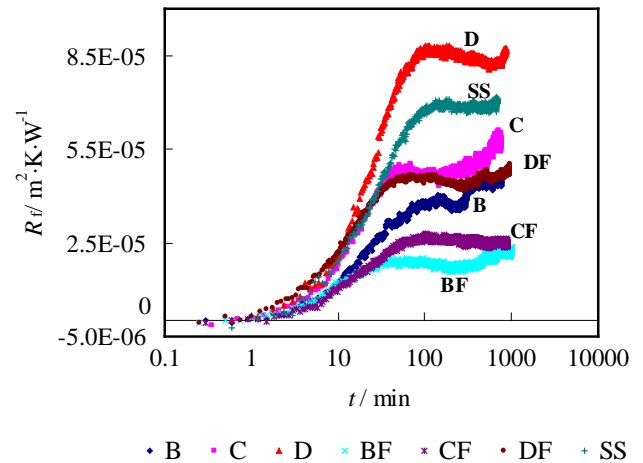


Fig. 6 Fouling curves on different disk surfaces at heat flux of $123.6 \text{ kW}\cdot\text{m}^{-2}$ and the initial calcium carbonate concentration of $250 \text{ mg}\cdot\text{L}^{-1}$

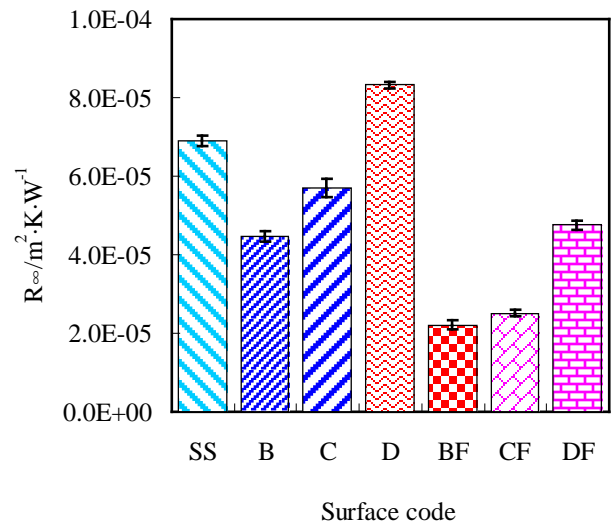


Fig. 7 Histogram of R_∞ on different heating surfaces categories (SS: AISI304 stainless steel; B, C, and D: TiO_2 coating; BF, CF, and DF: TiO_2 -FPS composite coating).

Figure 6 shows that the fouling resistance increases sharply at the initial period of the fouling test, and then remains almost constant. The fouling changing over time on all surfaces exhibits the law of the asymptotic fouling resistance curves. It could be seen that the asymptotic fouling resistance increases with the increase of the surface free energy as well as the surface roughness for the same surface material. The asymptotic fouling resistances of all the coated surfaces are less than that of the polished SS, except for the coating D surface. Large surface roughness and many TiO_2 particles with large sizes are observed on the coating D surface as shown in Fig. 1(e), which might serve as many crystal nucleuses for calcium carbonate

crystallization fouling. Meanwhile, the coating D has high surface free energy which also contributes to the high asymptotic fouling resistance. The SS surface has a high asymptotic fouling resistance because of its high surface free energy although it has very small surface roughness. In addition, the coating DF has a large asymptotic fouling resistance because it has very large surface roughness although its surface free energy decreases obviously compared with the coating D. The result indicates that the high surface roughness providing an increased number of nucleation sites for the crystallization process has overcome the contribution of the low surface energy that results in lower surface temperature. It is noteworthy that the asymptotic fouling resistance decreases markedly after the TiO₂ surface was treated with the hydrophobic FPS solution. This is because the reduced surface energy would lead to the decrease of the initial fouling rate and result in less deposit formation (Zettler et al., 2005).

It is noted that the negative fouling resistances are observed at the early stage of the fouling curves, as shown in Fig. 6. We found that a small amount of foulant had been deposited on the heat transfer surface before we heated the CaCO₃ solution to the saturated temperature in the boiling pool. These foulant deposited on the heat transfer surface might provide many nucleation sites for the bubble formation. Moreover, these additional nucleation sites increase the turbulence level in the zone near the heat transfer surface (Najibi et al., 1997), and therefore, the initial heat transfer coefficients might slightly higher than the average clean heat transfer coefficient we used at the initial stages of the fouling test.

Figure 8 shows the photograph of the fouling points shape on different boiling discs. Many fouling points are found after the fouling tests. They are the boiling sites where the crystallization crystals have formed and the steam bubbles have occurred during the pool boiling on these surfaces. Calcium carbonate is an inversely soluble salt and the temperature under the bubbles is higher than that at other positions of the disk surface. The fouling with a fairly high density and large adherence tendency are easily deposited under the bubbles. So a hard and whitish-colored fouling forms in the non-uniform regions where boiling nucleation occurs (region I in Fig. 8(a)) and a smooth, semitransparent fouling layer forms in the relatively undisturbed region between the boiling nucleation sites (region II). The loose fouling around each boiling nucleation site is found on the coating C surface, as shown in Fig. 8(b). Many small and fluffy fouling points are found on the coating CF as shown in Fig. 8(c). This result shows that a mass of bubbles with small departure diameters had been formed on this composite surface during pool boiling. In addition, the interaction between the fouling particles and the composite surface is poor because of its very low surface free energy; so the fouling is easily removed from the surface. Large size fouling points are found on the thick TiO₂ coating, as shown in Fig. 8(d). These fouling points might attribute to the big bubbles formed on this surface during the boiling. Since the pool boiling heat transfer on the disc has been probably blocked by the thick TiO₂ coating, a higher surface

temperature occurs and a denser, harder and more adherent fouling is formed on this surface.

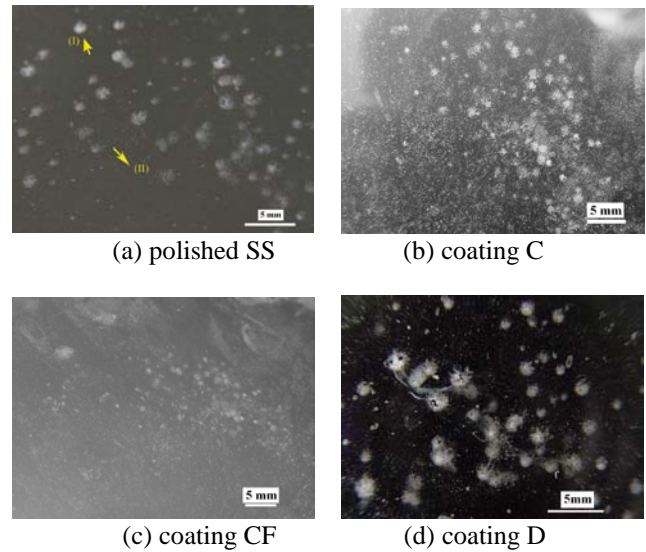


Fig. 8 Photograph of fouling appearance on different boiling discs.

The FE-SEM morphology and the energy dispersive X-ray spectroscopy (EDS) of the crystallization fouling on the coatings of C and CF are shown in Figs. 9 and 10.

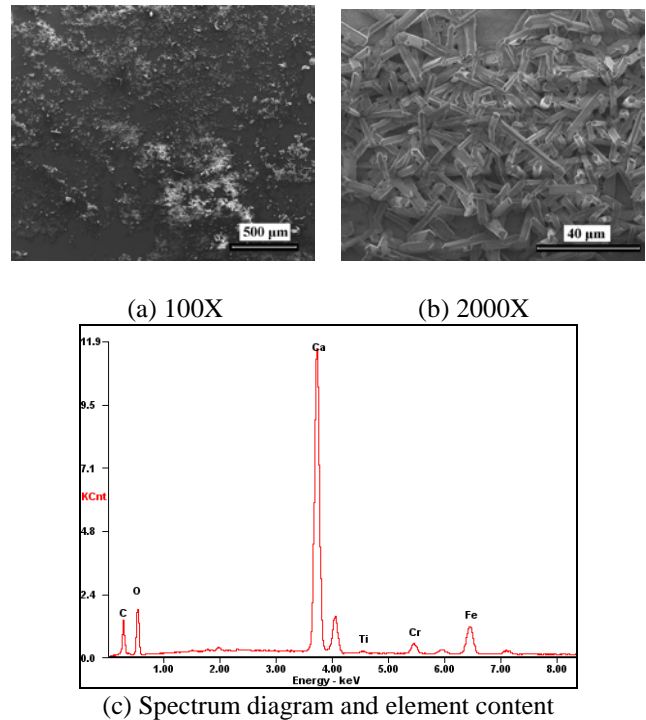


Fig. 9 FE-SEM and EDS of fouling layer on the coating C surface.

The six or five prismatic forms of the fouling crystals were accumulated on the coating C surface, as shown in Fig. 9(b). The fouling is very incompact, much fragile and easy to remove. The crystal form of this fouling is calcite (Tang et al., 2010). The lanceolate structure of the fouling is found on the coating CF surface, as shown in Fig. 10. The crystal

form of the fouling is aragonite (Tang et al., 2010) and easy to clean away. The amounts of the fouling crystals on the unit area of the coating CF surface are much less than that on the coating C. Meanwhile, the crystal size on the coating CF surface is much larger than that on the coating C, as shown in Fig. 9(b) and Fig. 10(b). The reasons for different crystal forms on the coatings of C and CF surface might be expressed as the following. On the CF surface, there are more small bubbles than on the C surface. Therefore, there are more nucleation sites on the CF surface than on the C surface. Under the bubbles, the temperature is higher than at the other positions on the surface. Because CaCO_3 is an inverse soluble salt, supersaturation is greater under the bubbles than at the other positions. According to literature, aragonite precipitates at higher supersaturations than calcite (Turner et al., 1998; Pääkkönen et al., 2009; Esawy et al., 2010). Therefore, the aragonite crystals were found on the CF surfaces and the calcite crystals on the C surfaces.

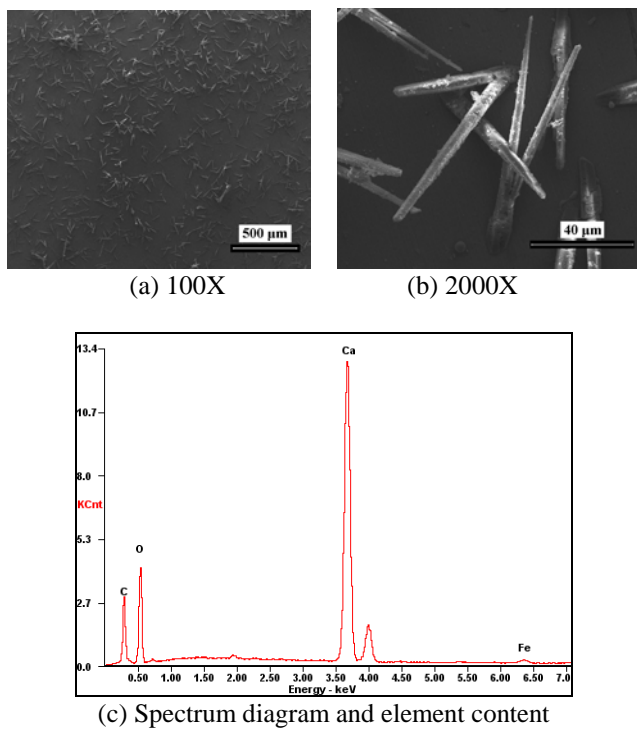


Fig. 10 FE-SEM and EDS of fouling layer on the coating CF surface

CONCLUDING REMARKS

The heat transfer coefficient of all the TiO_2 -FPS composite coatings increase compared with the TiO_2 coating with the same film thickness. The nucleation site density and the frequency of bubbles departure of the TiO_2 -FPS composite coating surface are far greater than that of the TiO_2 coating as well as of the polished 304 type stainless surface.

The asymptotic fouling resistance decreases markedly after the TiO_2 surface is treated with the hydrophobic FPS solution. Many small and fluffy fouling points are found on the TiO_2 -FPS composite coating surface. The fouling layer

on the TiO_2 -FPS composite surface is easy to remove. The calcite fouling crystals with six or five prismatic prism form accumulate on the thin TiO_2 coating surface. The lanceolate structure of the aragonite crystal fouling is found on the TiO_2 -FPS composite coating surface. In addition, the amount of the crystal fouling on the unit area of the composite coating is much less than on the TiO_2 coating with the same coating thickness. The hydrophobic TiO_2 -FPS composite coating exhibits a favorable pool boiling heat transfer performance as well as a preferable antifouling property.

NOMENCLATURE

D	diameter of the bubble, m
f	departure frequency of the bubble from the heat transfer surface, Hz
\dot{q}	heat flux, $\text{W}\cdot\text{m}^{-2}$
R_a	arithmetical mean deviation of profile, m
R	fouling resistance, $\text{m}^2\cdot\text{K}\cdot\text{W}^{-1}$
T	bulk solution temperature, K
t	time, s
greek symbols	
α	heat transfer coefficient, $\text{W}\cdot\text{m}^{-2}\cdot\text{K}^{-1}$
γ	surface free energy of the solid, $\text{J}\cdot\text{m}^{-2}$
abbreviation	
A, B, C, D	titania coating
BF, CD, DF	titania-fluoroalkylsilane composite coating
DLC	diamond like carbon
EDTA	ethylene-diamine-tetra-acetic acid
EDS	Energy dispersive X-ray spectroscopy
FE-SEM	Field emission scanning microscopy
FPS	fluoroalkylsilane
K-S	the designation of the nano-structured coating used in the literature (Malayeri et al., 2009)
LPD	liquid phase deposit
SS	AISI304 stainless steel
XPS	X-ray photoelectron spectroscopy
Subscript	
b	bulk
d	departure
f	fouled
g	growth time
s	surface
t	time
w	waiting time, or wall
∞	final state of fouling resistance

ACKNOWLEDGMENT

The authors are grateful to the National Natural Science Foundation of China (Grant numbers: 20876106) and Tianjin Research Program of Application Foundation and Advanced Technology (No.09JCZDJC24100) for the financial support. The authors thank Prof. Yang SR and Dr. Cao SX for their very valuable suggestions on the establishment of the pool boiling apparatus. The authors greatly acknowledge Pro. Puhakka, Eini for her good

suggestions for our explanations of different crystalline forms of CaCO_3 on the heat transfer surfaces. The authors also thank M.S. candidate Xu YG and Zhou WD for their help of the boiling bubbles video capture tests.

REFERENCES

- Al-Janabi, A., Malayeri, M.R., Müller-Steinhagen, H., 2011, Minimization of CaSO_4 deposition through surface modification, *Heat Transfer Engineering*, Vol. 32, pp. 291-299.
- Al-Janabi, A., Malayeri, M.R., Müller-Steinhagen, H., 2009, Minimization of CaSO_4 deposition through surface modification, *Proceedings of International Conference on Heat Exchanger Fouling and Cleaning VIII*, Schladming, Austria.
- Chu H., Yu B., 2009, A new comprehensive model for nucleate pool boiling heat transfer of pure liquid at low to high heat fluxes including CHF, *Int. J. Heat and Mass Transfer*, Vol. 52, pp. 4203-4210.
- Esawy, M., Abd-Elhady, M.S., Malayeri, M.R., Müller-Steinhagen, H., 2010, Influence of sintering on deposit formation during pool boiling of calcium sulphate solutions, *Experimental Thermal and Fluid Science*, Vol. 34, pp. 1439-1447.
- Jamialahmadi M., Blöchl R., Müller-Steinhagen H., 1989, Bubble dynamics and scale formation during boiling of aqueous calcium sulphate solutions, *Chemical Engineering and Processing: Process Intensification*, Vol. 26, pp. 15-26.
- Johnson M.A., De La Peña J., Mesler R.B., 1966, Bubble shapes in nucleate boiling, *AIChE J.*, Vol. 12, pp. 344-348.
- Lai, Y.K., Gao, X.F., Zhuang, H.F., Huang, J.Y., Lin, C.J., Jiang L., 2009, Designing super-hydrophobic porous nanostructures with tunable water adhesion, *Advanced Materials*, Vol. 21, pp. 3799-3803.
- Liang, H.S., Yang, W.J., 1998, Nucleate pool boiling heat transfer in a highly wetting liquid on micro-graphite-fiber composite surfaces, *Int. J. Heat and Mass Transfer*, Vol. 41, pp. 1993-2001.
- Malayeri, M.R., Al-Janabi, A., Müller-Steinhagen, H., 2009, Application of nano-modified surfaces for fouling mitigation, *Int. J. Energy Research*, Vol. 33, pp. 1101-1113.
- Michalski, M.C., Hardy, J., Saramago, B.J.V., 1998, On the surface free energy of PVC/EVA polymer blends: comparison of different calculation methods, *J. Colloid and Interface Science*, Vol. 208, pp. 319-328.
- Najibi S.H., Müller-Steinhagen H., Jamialahmadi M., 1997, Calcium carbonate scale formation during subcooled flow boiling, *J. Heat Transfer*, Vol. 119, pp. 767-775.
- Nishino, T., Meguro, M., Nakamae, K., Matsushita, M., Ueda, Y., 1999, The lowest surface free energy based on $-\text{CF}_3$ alignment, *Langmuir*, Vol. 15, pp. 4321-4323.
- Pääkkönen T.M., Riihimäki M., Puhakka E., Muurinen E., Simonson C.J., Keiski R.L., 2009, Crystallization fouling of CaCO_3 —effect of bulk precipitation on mass deposition on the heat transfer surface, *Proceedings of International Conference on Heat Exchanger Fouling and Cleaning VIII*, Schladming, Austria.
- Pioro I.L., Rohsenow W.M., Doerffer S.S., 2004, Nucleate pool-boiling heat transfer, I: review of parametric effects of boiling surface, *Int. J. Heat and Mass Transfer*, Vol. 47, pp.5033-5044.
- Rankin B.H., Adamson W.L., 1973, Scale formation as related to evaporator surface conditions, *Desalination*, Vol. 13, pp.63-87.
- Sermon, P.A., Leadley, J.G., 2004, Fluoroalkylsilane modification of sol-gel $\text{SiO}_2\text{-TiO}_2$ coatings, *J. Sol-Gel Science and Technology*, Vol. 32, pp. 293-296.
- Takata, Y., Hidaka, S., Uraguchi, T., 2006, Boiling feature on a super water-repellent surface, *Heat Transfer Engineering*, Vol. 27, pp. 25-30.
- Tang, Q.G., Meng, J.P., Liang, J.S., Nie L., Li Y.X., 2010, Effects of copper based alloys on the nucleation and growth of calcium carbonate scale, *J. Alloys and Compounds*, Vol. 491, pp. 242-247.
- Turner C.W., Smith D.W., 1998, Calcium carbonate scaling kinetics determined from radiotracer experiments with calcium-47, *Industrial & Engineering Chemistry Research*, Vol. 37, pp. 439-448.
- Wang, C.H., Dhir, V.K., 1993, Effect of surface wettability on active nucleation site density during pool boiling of water on a vertical surface, *J. Heat Transfer*, Vol. 115, pp. 659-669.
- Yu B.M., Cheng P. A fractal model for nucleate pool boiling heat transfer. *J. Heat Transfer*, 2002, 124(6):1117-1124.
- Wang, Y., Wang, L.L., Liu, M.Y., 2007, Antifouling and enhancing pool boiling by TiO_2 coating surface in nanometer scale thickness, *AIChE J.*, Vol. 53, pp. 3062-3076.
- Zettler, H.U., Wei, M., Zhao, Q., Müller-Steinhagen, H., 2005, Influence of surface properties and characteristics on fouling in plate heat exchangers, *Heat Transfer Engineering*, Vol. 26, pp. 3-17.
- Zhao, Q., Liu, Y., 2004, Investigation of graded Ni-Cu-P-PTFE composite coatings with anti-scaling properties, *Applied Surface Science*, Vol. 229, pp. 56-62.
- Zhao, Q., Wang, X., 2005, Heat transfer surfaces coated with fluorinated diamond-like carbon films to minimize scale formation, *Surface and Coatings Technology*, Vol. 192, pp. 77-80.
- Zhao, Q., Liu, Y., Wang, C., Wang, S., Müller-Steinhagen, H., 2005, Effect of surface free energy on the adhesion of bio-fouling and crystalline fouling, *Chemical Engineering Science*, Vol. 60, pp. 4858-4865.